

Supporting Information

**New reticular chemistry of pillared rare-earth kgd supermolecular
building layer frameworks with ethane-trapping property**

Hong-Xin Li,^a Han Fang,^a Yu-Feng Zhang,^a Zong-Hui Zhang,^a and Dong-Xu Xue*^a

^a Key Laboratory of Applied Surface and Colloid Chemistry, Ministry of Education, Xi'an Key Laboratory of Organometallic Material Chemistry, School of Chemistry & Chemical Engineering, Shaanxi Normal University, Xi'an 710062, China.

*E-mail: xuedx@snnu.edu.cn

Table of Contents

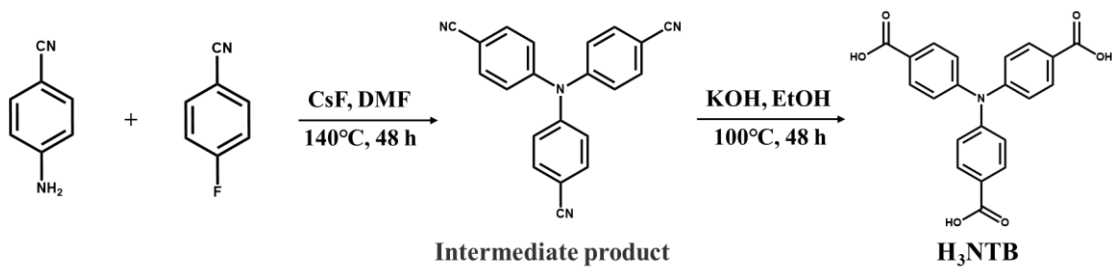
Section 1. Materials and General Procedures	2
Section 2. Additional Structural Figures	6
Section 3. Powder X-ray Diffraction (PXRD) patterns	9
Section 4. Thermal Gravimetric Analysis (TGA).....	10
Section 5. Low-Pressure Gas Sorption Measurements.....	11
Section 6. High-Pressure Methane Sorption Measurements.....	24
Section 7. Single Crystal X-ray Crystallography Data.....	26
Section 8. References	32

Section 1. Materials and General Procedures

All reagents were obtained from commercial sources and used without further purification. PXRD measurements were performed on a Rigaku MiniFlex 600 diffractometer with Cu $K\alpha$ ($\lambda = 1.5406 \text{ \AA}$), and the X-ray tube was operated at 40 kV and 40 mA. High-resolution thermogravimetric analysis (TGA) was performed under a continuous N₂ flow and recorded on a Q600SDT thermal analyzer with a heating rate of 5 °C/min. Fourier transform infrared (FT-IR) spectrum (400-4000 cm⁻¹, KBr pellet) was collected in the solid state on a Bruker Tensor 27 FT-IR spectrometer. Elemental analyses (C, H, N and S) were obtained from a Vario EL cube analyzer. Breakthrough system used in this work is the homemade HPMC41 gas separation test system (Nanjing Hope Analytical Equipment Co., Ltd).

Synthesis of ligands

Synthesis of H₃NTB

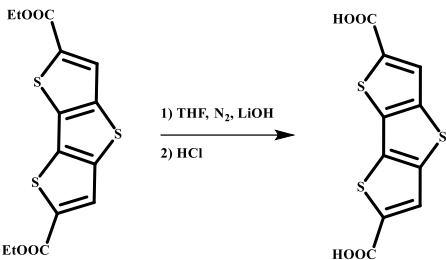


4,4',4"-nitritotribenzoic acid (H₃NTB) was synthesized according to the previously reported literature.¹

In the first step, 1.18g (10 mmol) of 4-aminobenzonitrile was dissolved in 50 mL N,N-dimethylformamide (DMF). Then 6.04 g (40.0 mmol) of CsF was added slowly to the solution with continuous stirring followed by the addition of 2.66 g (22 mmol) of 4-fluorobenzonitrile. The total reaction mixture was then refluxed at 140 °C for 48 h. After cooling, the reaction mixture was poured into ice cold water to precipitate out the intermediate product (4,4',4"-tricyanotriphenylamine). The precipitate was filtered and washed with plenty of water and finally dried in a hot air oven to yield 2.94 g (91%) of 4,4',4"-tricyanotriphenylamine.

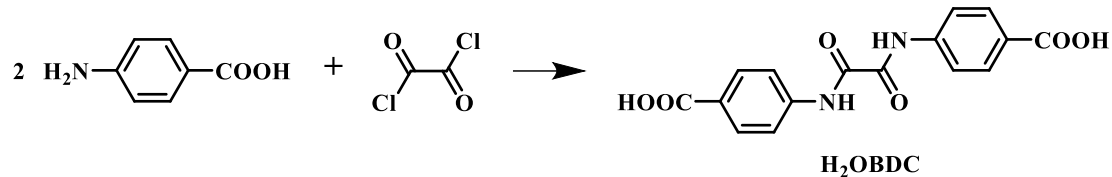
In the second step, 2 g of 4,4',4"-tricyanotriphenylamine was dissolved in a mixture containing 20 mL ethanol and 60 mL 6M KOH solution. The mixture was then refluxed at 100 °C for 48 h. After cooling down to room temperature the mixture was acidified with 3M HCl. The pH of the solution was adjusted to 3 to get a white precipitate. Finally the precipitate was filtered and washed with plenty of water, dried in an oven to obtain the H₃NTB product (2.1 g, ~90%). The finally product was used without further purification. ¹H NMR (400 MHz, DMSO-*d*₆): δ = 7.91 (d, 6H), 7.15 (dd, 6 H) ppm.

Synthesis of H₂DTTDC



Dithieno[3,2-b:2',3'-d] thiophene-2,6-dicarboxylic acid diethyl ester (5.00 g, 14.7 mmol) was suspended in tetrahydrofuran (75 mL). An aqueous solution of 1 M lithium hydroxide (75 mL, 75 mmol, 5.1 equiv.) was added, causing the color of the suspension to change from yellow to terracotta. The mixture was heated to 70 °C and followed by stirring at this temperature for 4 h, and then afforded an orange solution. The solvent was evaporated on a rotary evaporator until the volume remaining was about 75 mL. A small amount of precipitate was observed. The solution was acidified with 1 M hydrochloric acid (100 mL) to give a white precipitate with some slight foam. The solid was filtered slowly under vacuum on a Büchner funnel and washed sequentially with water (200 mL), methanol (100 mL) and diethyl ether (100 mL). Finally, the solid was dried overnight in a high vacuum oven (40 °C, approx. 0.02 mmHg) to afford the crude diacid (H₂DTTDC) (3.8 g, 91%). The ligand was used without further purification. ¹H NMR (400 MHz, DMSO-*d*₆): δ: 8.18 ppm (s, 2 H).

Synthesis of H₂OBDC



H₂OBDC was synthesized according to the previously reported procedure with slight modification.² 4-aminobenzoic acid (1.28 g, 8.37 mmol) was dissolved in NMP (15 mL) and cooled to 5 °C in ice bath. Liquid oxalyl chloride (0.812 g, 4.00 mmol) was added drop wise over 1 h. The reaction mixture was stirred at 5 °C for 2 h followed by continue stirring at room temperature for an additional 12 h. After that, 20 mL of distilled water was added to the reaction. The product was filtered and washed with NMP (20 mL), distilled water (5 × 50 mL), methanol (2 × 20 mL). The product was then dried at 65 °C for 12 h to afford the H₂OBDC linker as a light grey powder (1.10 g, 84%). ¹H NMR (400 MHz, DMSO-*d*₆): δ = 11.09 (s, 2H), 7.74 (dd, 4H), 7.55 (dd, 4H) ppm.

Synthesis of MOFs

Synthesis of Tb-NTB-HNTB

A mixture of Tb(NO₃)₃·6H₂O (19.7 mg, 0.0435 mmol), H₂BPDC (5.3 mg, 0.02175 mmol), H₃NTB (8.2 mg, 0.02175 mmol) and DMF (3.0 mL) and 2-FBA (FBA = 2-fluorobenzoic acid, 0.6 mL, 3.48 M/DMF) were combined in a 20 mL scintillation

vial, sealed and heated to 115 °C for 24 h. The colorless polyhedral crystals were collected, washed with DMF, and then air-dried. Yield ≈ 56.0% (based on H₃NTB). Selected IR (KBr, cm⁻¹): 3307 (br), 3070 (w), 2934 (w), 1664 (s), 1592 (vs), 1541 (m), 1405 (vs), 1278 (w), 1177 (s), 1101 (m), 1012 (w), 855 (m), 787 (s), 707 (m), 673 (m), 571 (w), 525 (w). Elem. Anal. (%) Calcd for C₉₄H₁₀₈F₈N₈O₄₁Tb₆: C, 36.29; H, 3.50; N, 3.60. Found: C, 36.29; H, 3.83; N, 3.86.

Synthesis of Tb-NTB-BDC

A mixture of Tb(NO₃)₃·6H₂O (19.7 mg, 0.0435 mmol), H₂BDC (8.3 mg, 0.05 mmol), H₃NTB (7.5 mg, 0.02 mmol), DMF (3.0 mL), 2-FBA (FBA = 2-fluorobenzoic acid, 0.6 mL, 3.48 M/DMF), acetic acid (100 μL) and n-pentanol (0.5 mL) were combined in a 20 mL scintillation vial, sealed and heated to 115 °C for 24 h. The colorless hexagonal prism crystals were collected, washed with DMF, and then air-dried. Yield ≈ 79.0% (based on H₃NTB). Selected IR (KBr, cm⁻¹): 3383 (br), 3070 (w), 2934 (w), 1660 (s), 1596 (vs), 1507 (w), 1402 (vs), 1312 (m), 1273 (w), 1177 (m), 1101 (m), 1016 (m), 859 (w), 787 (m), 753 (m), 711 (w), 669 (m), 571 (w), 521 (m), 444 (m). Elem. Anal. (%) Calcd for C₈₅H₁₁₇F₈N₉O₄₄Tb₆: C, 33.21; H, 3.84; N, 4.10. Found: C, 33.13; H, 4.45; N, 4.52.

Synthesis of Tb-NTB-1,4-NDC

A mixture of Tb(NO₃)₃·6H₂O (19.7 mg, 0.087 mmol), 1,4-H₂NDC (10.8 mg, 0.05 mmol), H₃NTB (7.5 mg, 0.02 mmol), DMF (3.0 mL) and 2-FBA (FBA = 2-fluorobenzoic acid, 0.5 mL, 3.48 M/DMF), acetic acid (100 μL) and n-pentanol (0.5 mL) were combined in a 20 mL scintillation vial, sealed and heated to 115 °C for 24 h. The colorless hexagonal prism crystals were collected, washed with DMF, and then air-dried. Yield ≈ 69.0% (based on H₃NTB). Selected IR (KBr, cm⁻¹): 3374 (br), 3069 (w), 2934 (w), 1664 (s), 1592 (vs), 1550 (w), 1397 (vs), 1317 (m), 1266 (m), 1177 (m), 1101 (m), 864 (m), 826 (m), 792 (s), 711 (w), 665 (w), 626 (w), 550 (m), 441 (w). Elem. Anal. (%) Calcd for C₁₀₀H₁₇₂F₈N₁₀O₆₆Tb₆: C, 32.69; H, 4.66; N, 3.81. Found: C, 32.42; H, 4.72; N, 4.02.

Synthesis of Tb-NTB-DTTDC

A mixture of Tb(NO₃)₃·6H₂O (19.7 mg, 0.0435 mmol), H₂DTTDC (6.2 mg, 0.02175 mmol), H₃NTB (8.2 mg, 0.02175 mmol), DMA (3.0 mL) and 2-FBA (FBA = 2-fluorobenzoic acid, 0.6 mL, 3.48 M/DMF) were combined in a 20 mL scintillation vial, sealed and heated to 115 °C for 24 h. The colorless hexagonal prism crystals were collected, washed with DMF, and then air-dried. Yield ≈ 54.0% (based on H₃NTB). Selected IR (KBr, cm⁻¹): 3199 (br), 3089 (w), 2938 (w), 1660 (vs), 1596 (s), 1554 (m), 1504 (s), 1403 (vs), 1318 (w), 1273 (w), 1171 (m), 1099 (m), 1013 (w), 862 (m), 782 (s), 671 (m), 5789 (m), 520 (w), 443 (w). Elem. Anal. (%) Calcd for C₈₈H₁₀₆F₈N₈O₄₄S₉Tb₆: C, 31.33; H, 3.17; N, 3.32, S, 8.55. Found: C, 31.62; H, 3.54; N, 2.90; S, 8.19.

Synthesis of Tb-NTB-OBDC

A mixture of Tb(NO₃)₃·6H₂O (19.4 mg, 0.0435 mmol), H₂OBDC (6.7 mg, 0.05

mmol), H₃NTB (7.5 mg, 0.02 mmol), DMF (3.0 mL), 2-FBA (FBA = 2-fluorobenzoic acid, 0.6 mL, 3.48 M/DMF) and acetic acid (100 μ L) were combined in a 20 mL scintillation vial, sealed and heated to 115 °C for 12 h. The colorless hexagonal prism crystals were collected, washed with DMF, and then air-dried. Yield \approx 65.0% (based on H₃NTB). Selected IR (KBr, cm⁻¹): 3594(br), 3239(br), 2930(w), 1664(s), 1596(s), 1495(m), 1402(vs), 1312(m), 1281(w), 1173(w), 1096(m), 982(w), 830(w), 787(s), 732(w), 707(m), 669(m), 571(m), 529(w), 449(w). Elel. Anal. (%) Calcd for C₁₁₂H₁₄₄F₈N₁₆O₅₂Tb₆: C, 36.76; H, 4.05; N, 6.34. Found: C, 36.92; H, 4.30; N, 6.61.

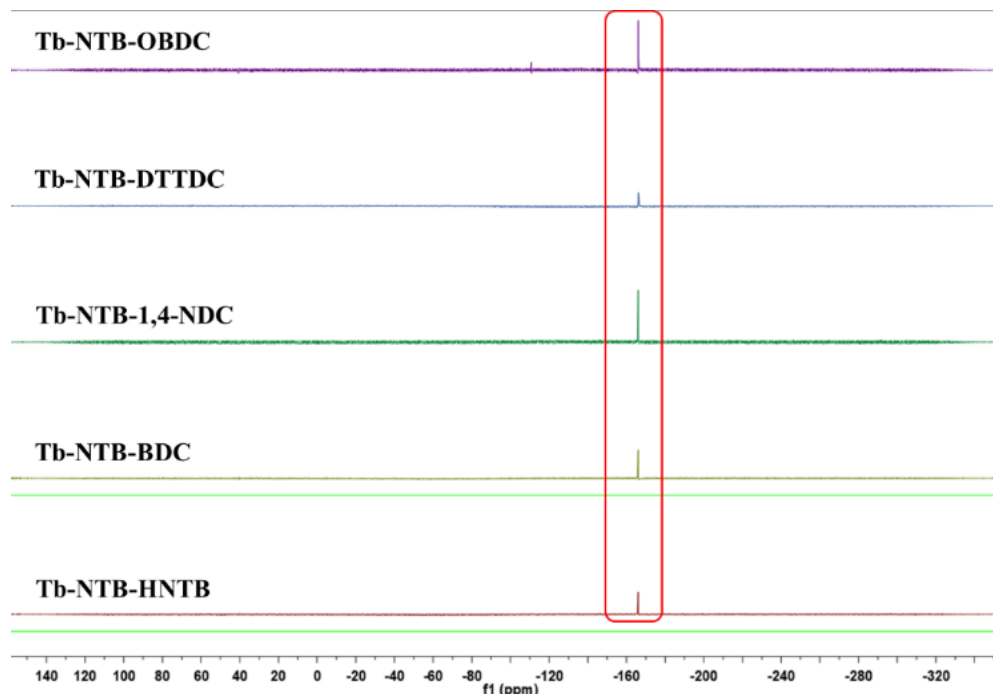


Fig. S1 The ¹⁹F NMR (400 MHz, DMSO-*d*₆) spectra of Tb-NTB-HNTB, Tb-NTB-BDC, Tb-NTB-1,4-NDC, Tb-NTB-DTTDC and Tb-NTB-OBDC. For all materials, there is a peak at δ = -166 ppm, this signal is attributed to HF, from the dissolved materials in H₂SO₄ and DMSO-*d*₆.

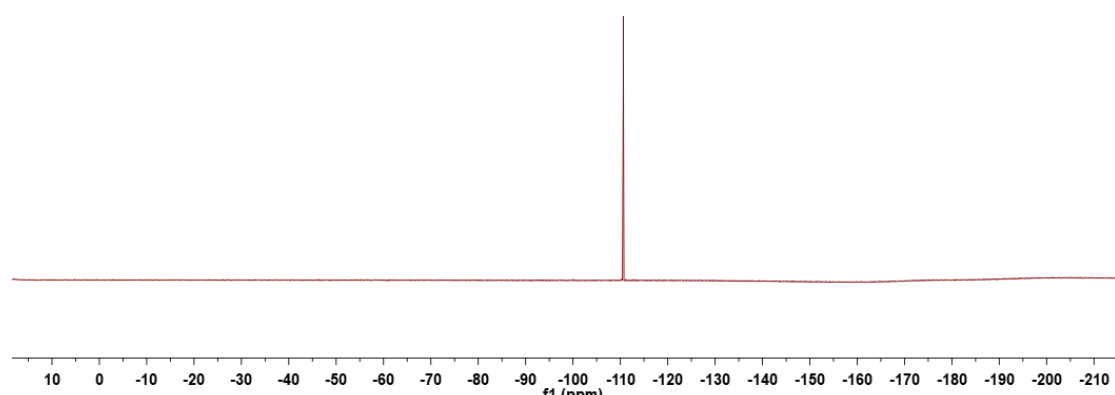


Fig. S2 The ¹⁹F NMR (400 MHz, DMSO-*d*₆) spectra of 2-fluorobenzoic acid, it has a peak at δ = -110 ppm.

Section 2. Additional Structural Figures

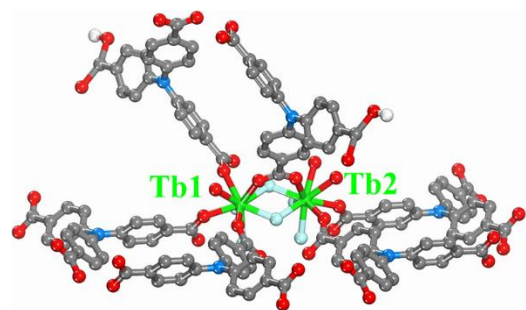


Fig. S3 The coordination environment of the rare earth metal ions in Tb-NTB-HNTB.

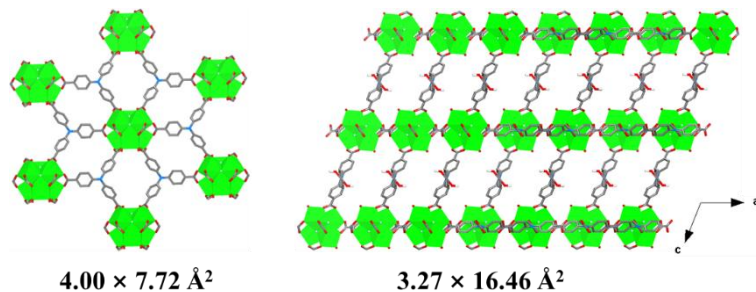


Fig. S4 Channels in Tb-NTB-HNTB along different directions with their sizes.

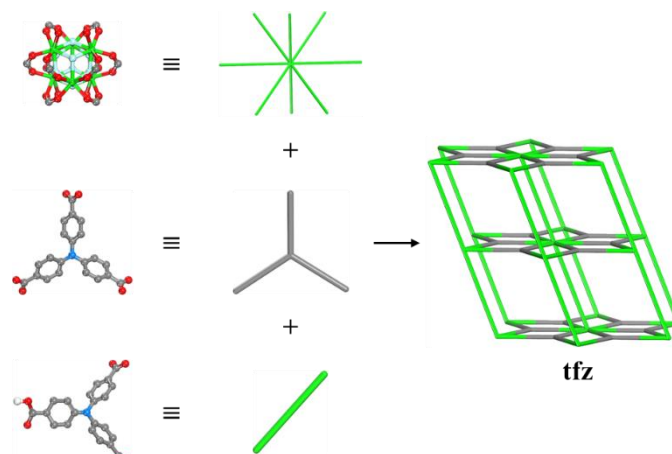


Fig. S5 Topology analysis of Tb-NTB-HNTB based on the node-linker strategy.

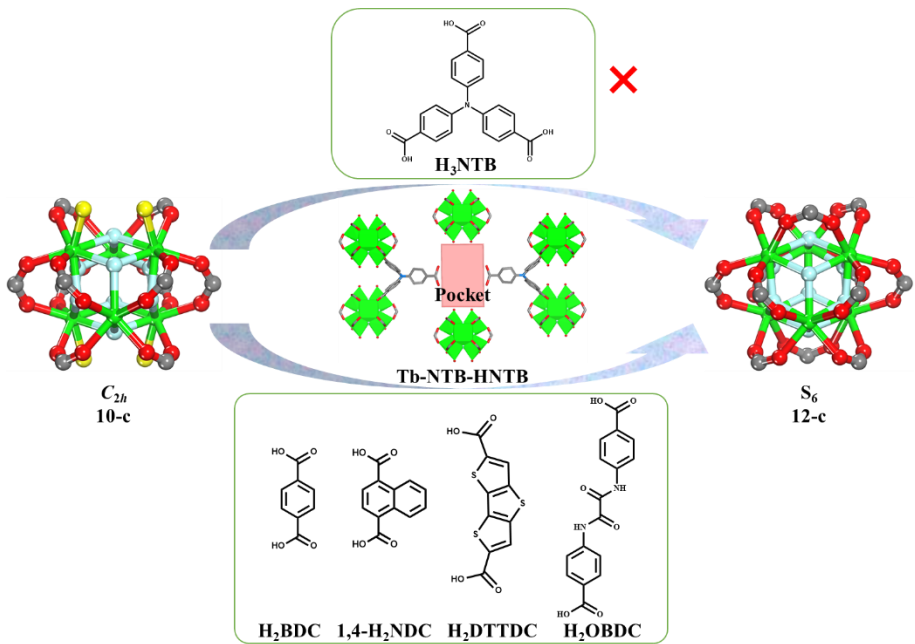


Fig. S6 Schematic representation of HNTB pillar in $Tb\text{-NTB-HNTB}$ replaced by different ditopic ligands.

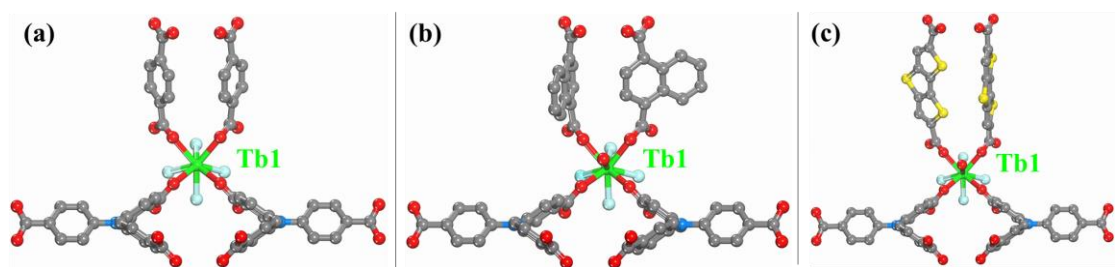


Fig. S7 The coordination environments of the rare earth metal ions in (a) $Tb\text{-NTB-BDC}$, (b) $Tb\text{-NTB-1,4-NDC}$ and (c) $Tb\text{-NTB-DTTDC}$.

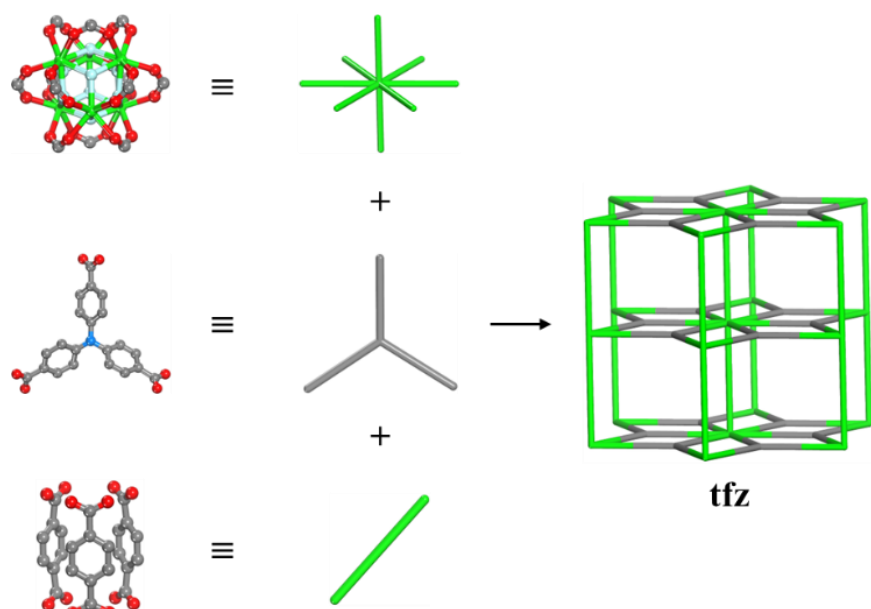


Fig. S8 Topology analysis of $Tb\text{-NTB-BDC}$ based on the node-linker strategy.

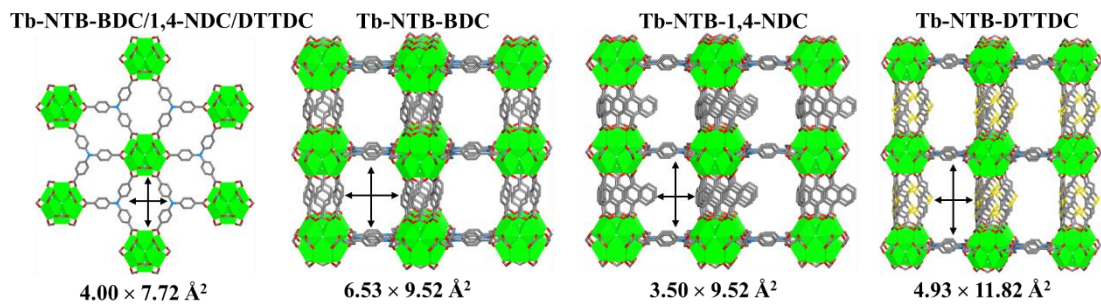


Fig. S9 One-dimensional channels with their sizes in Tb-NTB-BDC, Tb-NTB-1,4-NDC and Tb-NTB-DTTDC.

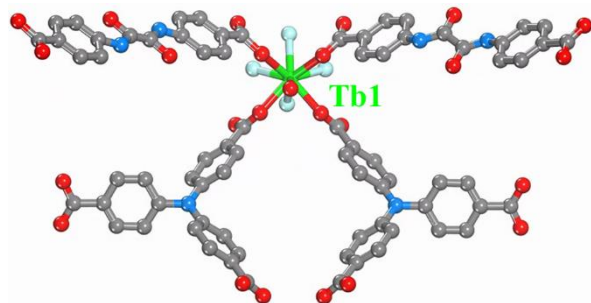


Fig. S10 The coordination environment of the rare earth metal ion in Tb-NTB-OBDC.

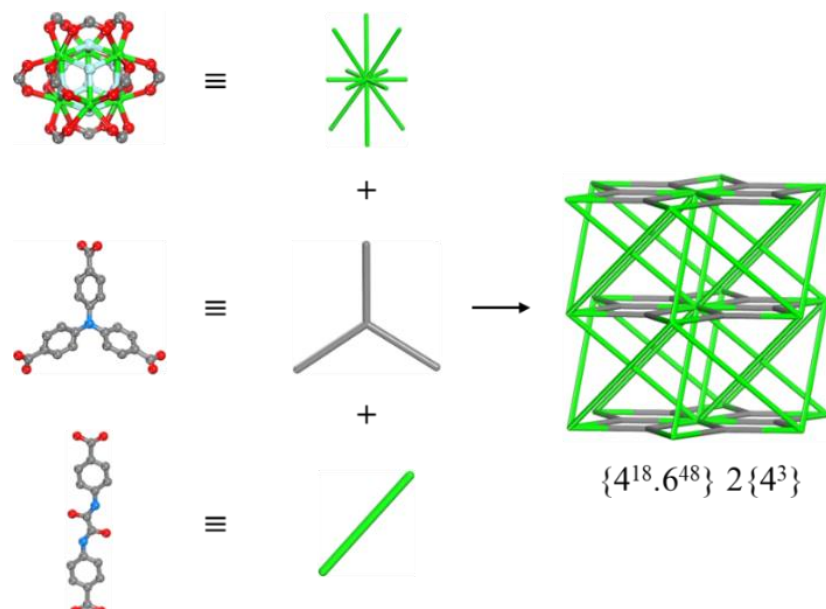


Fig. S11 Topology analysis of Tb-NTB-OBDC based on the node-linker strategy.

Section 3. Powder X-ray Diffraction (PXRD) patterns

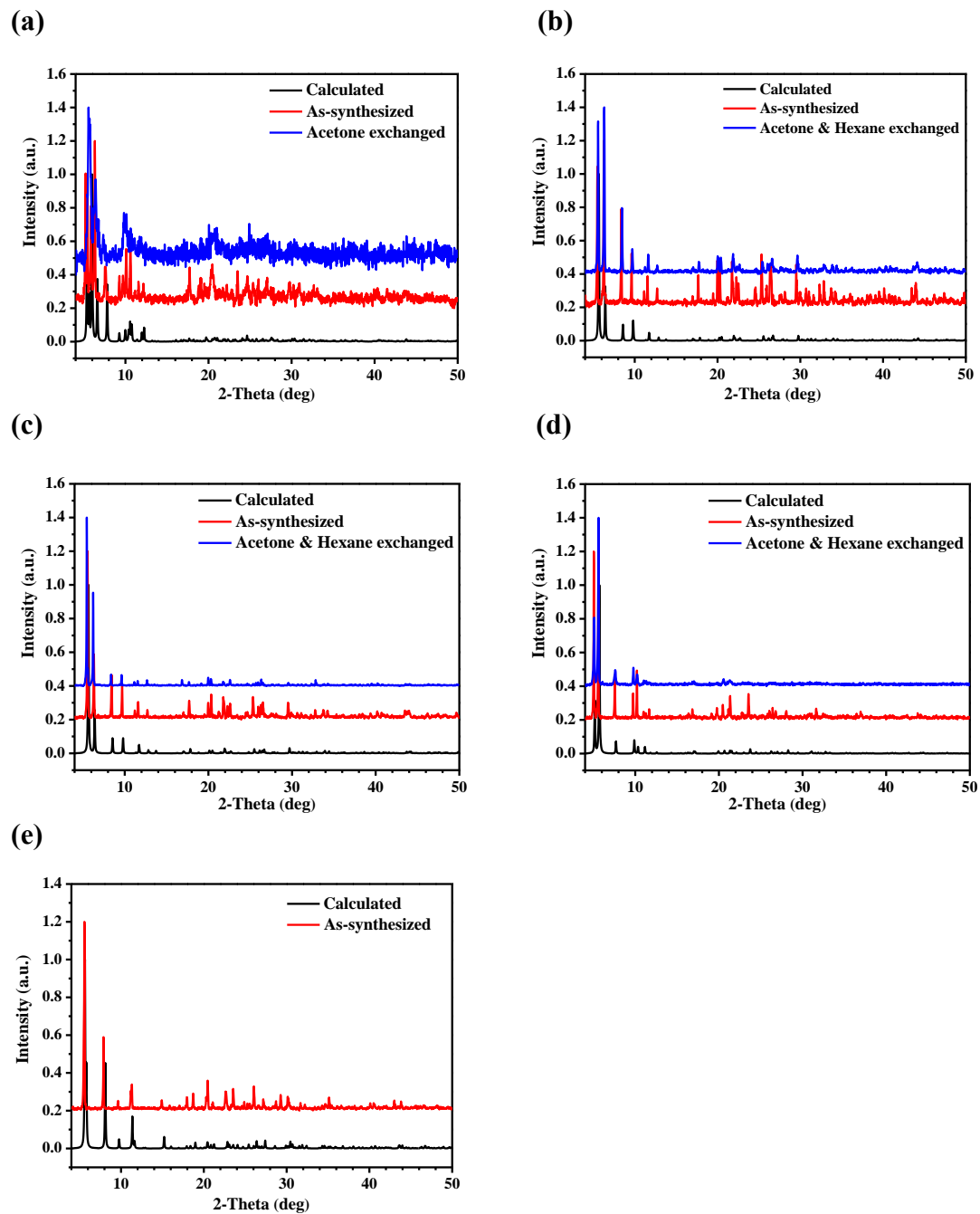


Fig. S12 Powder X-ray diffraction patterns of (a) Tb-NTB-HNTB, (b) Tb-NTB-BDC, (c) Tb-NTB-1,4-NDC, (d) Tb-NTB-DTTDC and (e) Tb-NTB-OBDC.

Section 4. Thermal Gravimetric Analysis (TGA)

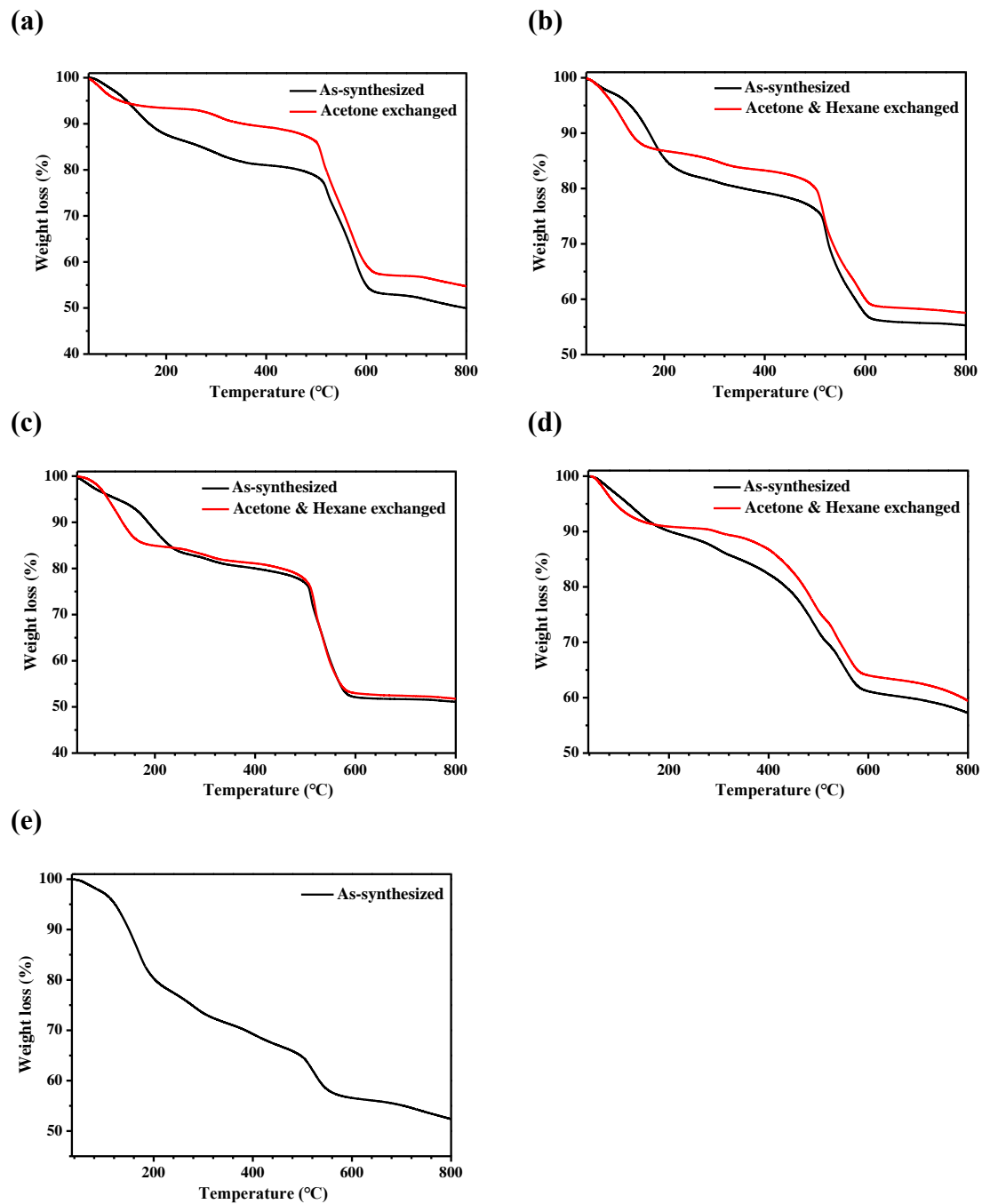


Fig. S13 TGA plots of (a) Tb-NTB-HNTB, (b) Tb-NTB-BDC, (c) Tb-NTB-1,4-NDC, (d) Tb-NTB-DTTDC and (e) Tb-NTB-OBDC.

Section 5. Low-Pressure Gas Sorption Measurements

Low pressure gas sorption studies were conducted on a fully automated micropore gas analyzer Autosorb-iQ3 (Quantachrome Instruments) at relative pressures up to 1 atm. The cryogenic temperature was controlled using liquid nitrogen at 77 K. The bath temperature for the C₂H₆, C₂H₄, C₂H₂ and CO₂ sorption measurements was controlled using a recirculating bath containing an ethylene glycol/H₂O mixture. The apparent surface areas were determined from the nitrogen adsorption isotherms collected at 77 K by applying the BET models. Pore size analyses were performed using a cylindrical/spherical NLDFT pore model system by assuming an oxidic (zeolitic) surface.

The calculation methods of adsorption enthalpy:

- (1) The isosteric enthalpy of adsorption, Q_{st} was determined by fitting the adsorption isotherms at 273 and 298 K to the Single-site Langmuir equation (Eqn 1);

$$n = \frac{n_L bp}{1+bp} \quad (1)$$

Where n is the amount of gas adsorbed in mmol/g, P is the pressure in Pa, n_L is the saturation capacity in mmol/g, and b is the Langmuir parameter of adsorption site.

Using the Single-site Langmuir equation fit, the isosteric heat of adsorption can be calculated for the material as a function of the total amount of gas adsorbed using the Clausius-Clapeyron equation (Eqn 2).

$$\frac{dlnp}{dT} = \frac{\Delta H}{nRT^2} = \frac{\Delta_r H_m}{RT^2} \quad (2)$$

- (2) Q_{st} was determined by fitting the adsorption isotherms at 273 and 298 K to the Dual-site Langmuir equation (Eqn 3);

$$n = \frac{n_{L,A} b_A p}{1+b_A p} + \frac{n_{L,B} b_B p}{1+b_B p} \quad (3)$$

Where n is the amount of gas adsorbed in mmol/g, P is the pressure in Pa, $n_{L,A}$ and $n_{L,B}$ are the saturation capacity in mmol/g, and b_A and b_B are the Langmuir parameter of adsorption sites 1 and 2.

Using the Dual-site Langmuir equation fit, the isosteric heat of adsorption can be calculated for the material as a function of the total amount of gas adsorbed using the Clausius-Clapeyron equation (Eqn 2).

- (3) Q_{st} was determined by fitting the adsorption isotherms at 273 and 298 K to the Langmuir-Freundlich equation (Eqn 4);

$$n = \frac{n_L b p^{\frac{1}{t}}}{1+b p^{\frac{1}{t}}} \quad (4)$$

Where n is the amount of gas adsorbed in mmol/g, P is the pressure in Pa, n_L is the saturation capacity in mmol/g, and b is the Langmuir parameter of adsorption site, and t represent the number of the adsorption sites.

Using the Langmuir-Freundlich equation fit, the isosteric heat of adsorption can be calculated for the material as a function of the total amount of gas adsorbed using the

Clausius-Clapeyron equation (Eqn 2).

(4) Q_{st} was determined by fitting the adsorption isotherms at 273 and 298 K to the Toth equation (Eqn 5);

$$n = \frac{n_L bp}{[1 + (bp)t]^{1/t}} \quad (5)$$

Where n is the amount of gas adsorbed in mmol/g, P is the pressure in Pa, n_L is the saturation capacity in mmol/g, and b is the Langmuir parameter of adsorption site, and t represent the inhomogeneity of the adsorbed surface.

Using the Langmuir-Freundlich equation fit, the isosteric heat of adsorption can be calculated for the material as a function of the total amount of gas adsorbed using the Clausius-Clapeyron equation (Eqn 2).

(5) Q_{st} was determined by fitting the adsorption isotherms at 273 and 298 K to the virial 2 equation (Eqn 6);

$$\ln P = \ln(N) + \left(\frac{1}{T}\right) \sum_{i=0}^m a_i \times N_i + \sum_{j=0}^n b_i \times N_i \quad (6)$$

Where N is the amount of gas adsorbed in mmol/g, P is the pressure in Pa, a_i and b_j are the empirical constant, and T is the temperature in K.

Using the virial 2 equation fit, the isosteric heat of adsorption can be calculated for the material as a function of the total amount of gas adsorbed using the Clausius-Clapeyron equation (Eqn 2).

IAST calculation of adsorption selectivity:

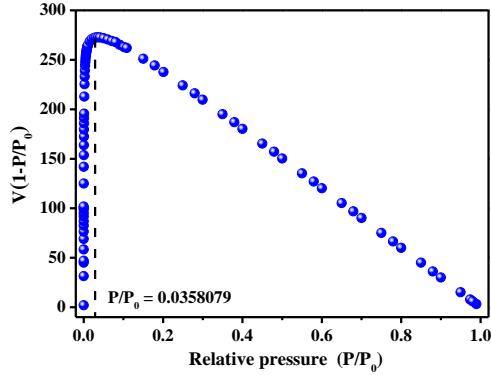
IAST (Ideal Adsorption Solution Theory) was used to predict binary mixture adsorption from the experimental pure gas isotherms.³⁻⁵ In order to perform the integrations required by IAST, the single-component isotherms should be fitted by a proper model. In practice, several methods to do this are available. We found for this set of data that the dual-site Langmuir-Freundlich equation (Eqn 7) was successful in fitting the data. As can be seen in Figure S28-31 and Table S8-11, the model fits the isotherms very well ($R^2 > 0.9999$).

$$q = \frac{q_{m,1} b_1 p^{1/n_1}}{1 + b_1 p^{1/n_1}} + \frac{q_{m,2} b_2 p^{1/n_2}}{1 + b_2 p^{1/n_2}} \quad (\text{Eqn 7})$$

Herein, P is the pressure of the bulk gas at equilibrium with the adsorbed phase (kPa), q is the adsorbed amount per mass of adsorbent (mmol/g), $q_{m,1}$ and $q_{m,2}$ are the saturation capacities of sites 1 and 2 (mmol/g), b_1 and b_2 are the affinity coefficients of sites 1 and 2 (1/kPa), and n_1 and n_2 represent the deviations from an ideal homogeneous surface. The fitted parameters were then used to predict multicomponent adsorption with IAST.

The selectivity $S_{A/B}$ in a binary mixture of components A and B is defined as $(x_A/y_A)/(x_B/y_B)$, where x_i and y_i are the mole fractions of component i ($i = A, B$) in the adsorbed and bulk phases, respectively

(a)



(b)

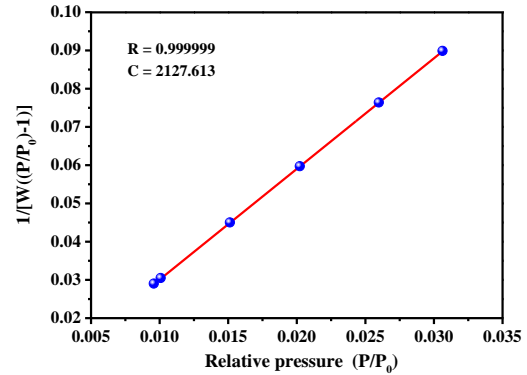
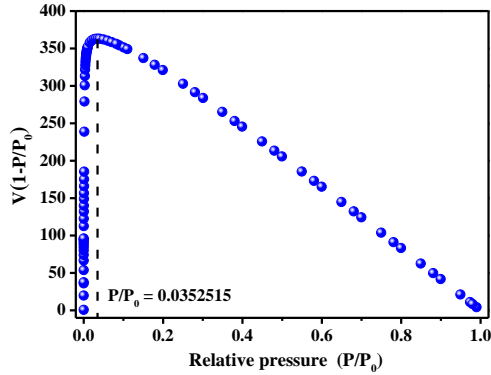


Fig. S14 (a) $V(1-P/P_0)$ vs. P/P_0 for Tb-NTB-HNTB, only the range below $P/P_0 = 0.035$ satisfies the first consistency criterion for applying the BET theory and (b) plot of the linear region for the BET equation.

(a)



(b)

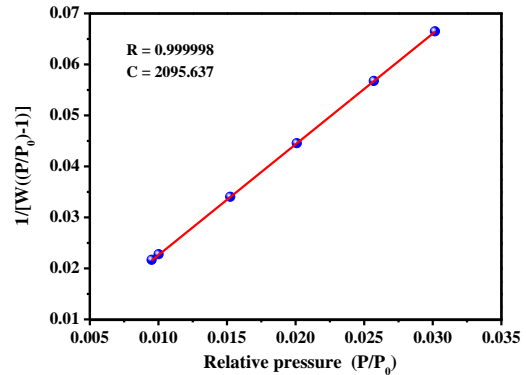
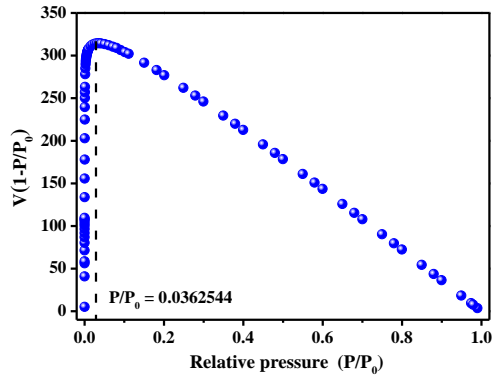


Fig. S15 (a) $V(1-P/P_0)$ vs. P/P_0 for Tb-NTB-BDC, only the range below $P/P_0 = 0.035$ satisfies the first consistency criterion for applying the BET theory and (b) plot of the linear region for the BET equation.

(a)



(b)

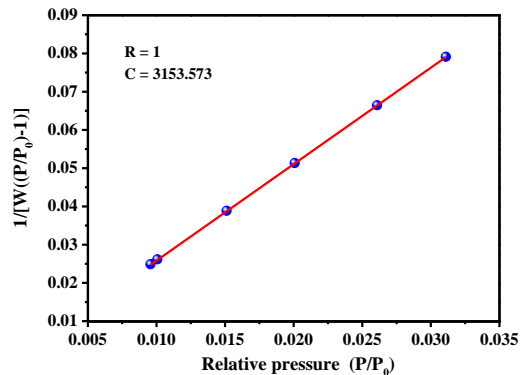
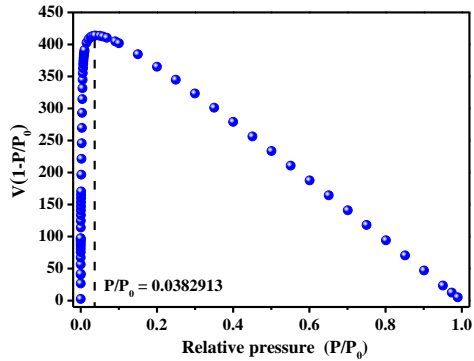


Fig. S16 (a) $V(1-P/P_0)$ vs. P/P_0 for Tb-NTB-1,4-NDC, only the range below $P/P_0 = 0.036$ satisfies the first consistency criterion for applying the BET theory and (b) plot of the linear region for the BET equation.

(a)



(b)

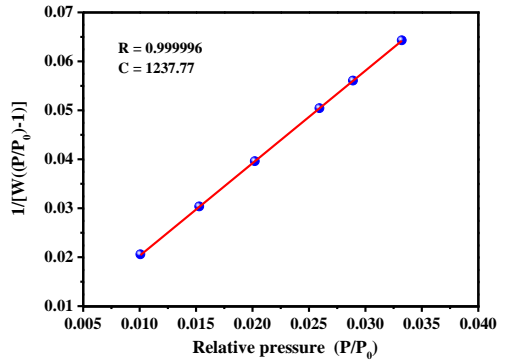
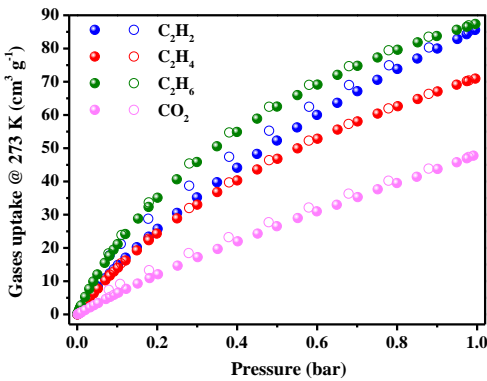
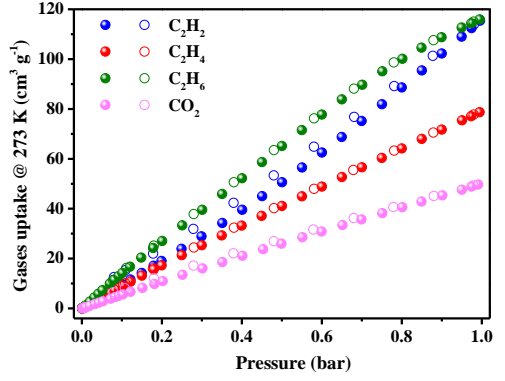


Fig. S17 (a) $V(1-P/P_0)$ vs. P/P_0 for Tb-NTB-DTTDC, only the range below $P/P_0 = 0.038$ satisfies the first consistency criterion for applying the BET theory and (b) plot of the linear region for the BET equation.

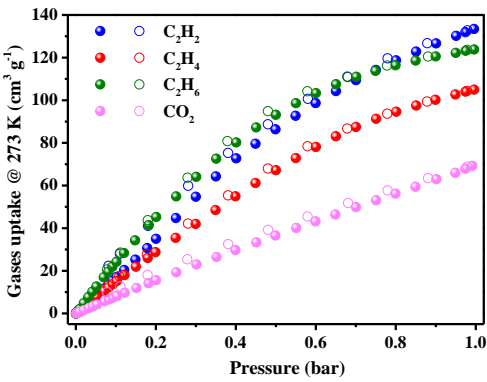
(a)



(b)



(c)



(d)

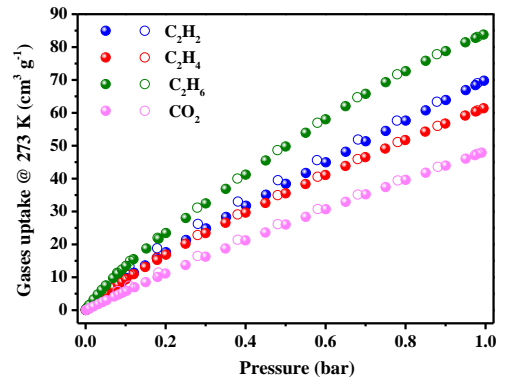


Fig. S18 Pure component sorption isotherms of different gases for (a) Tb-NTB-HNTB, (b) Tb-NTB-BDC, (c) Tb-NTB-1,4-NDC and (d) Tb-NTB-DTTDC at 273 K, respectively.

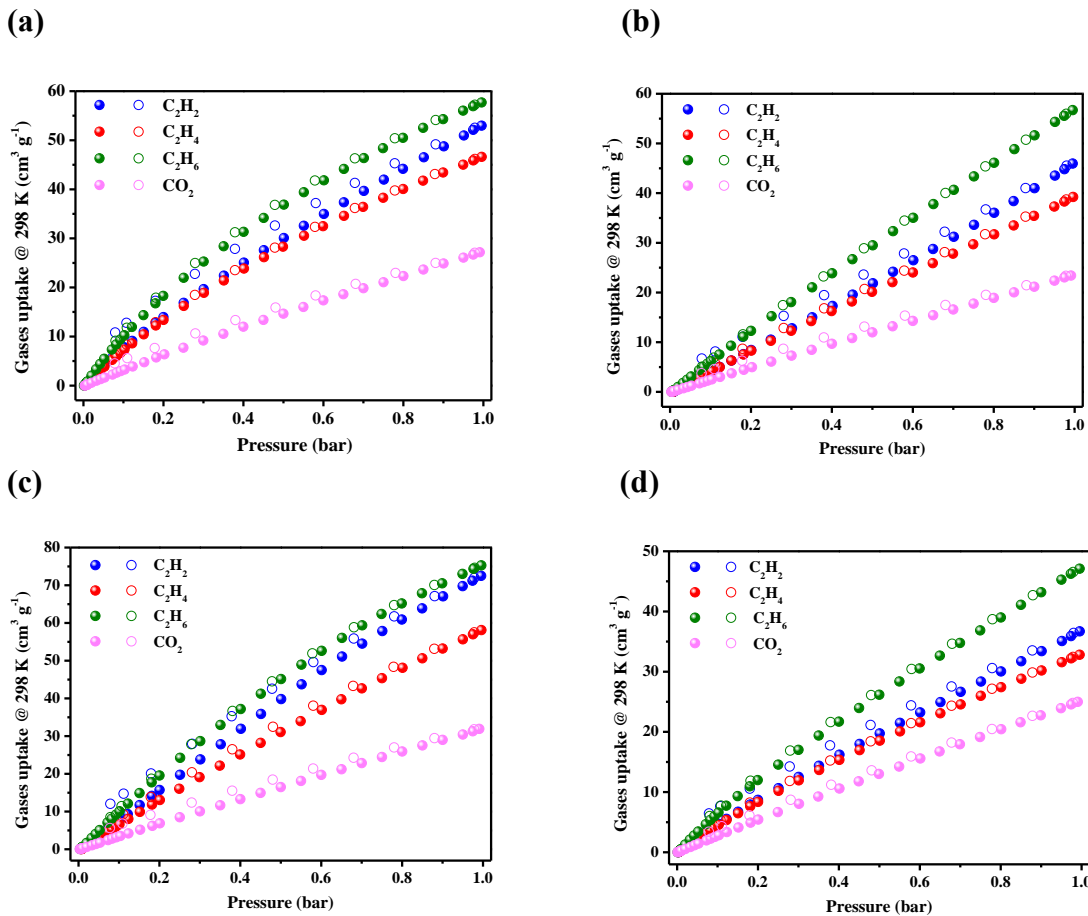


Fig. S19 Pure component sorption isotherms of different gases for (a) Tb-NTB-HNTB, (b) Tb-NTB-BDC, (c) Tb-NTB-1,4-NDC and (d) Tb-NTB-DTTDC at 298 K, respectively.

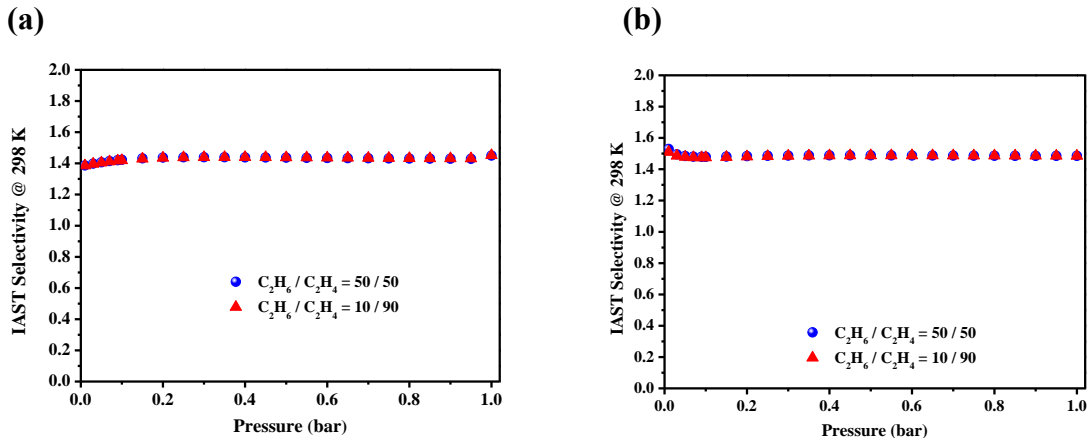


Fig. S20 IAST selectivity of (a) Tb-NTB-HNTB and (b) Tb-NTB-BDC under different ethane/ethylene ratios.

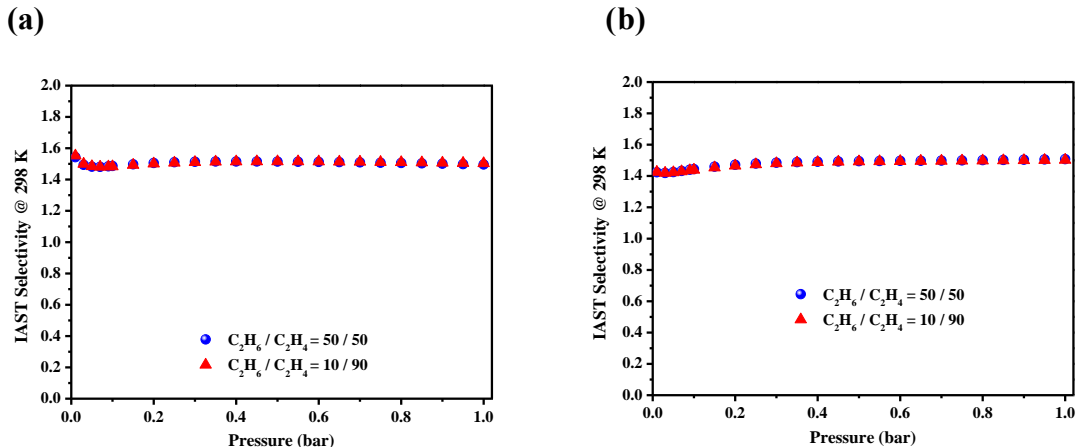


Fig. S21 IAST selectivity of (a) Tb-NTB-1,4-NDC and (b) Tb-NTB-DTTDC under different ethane/ethylene ratios.

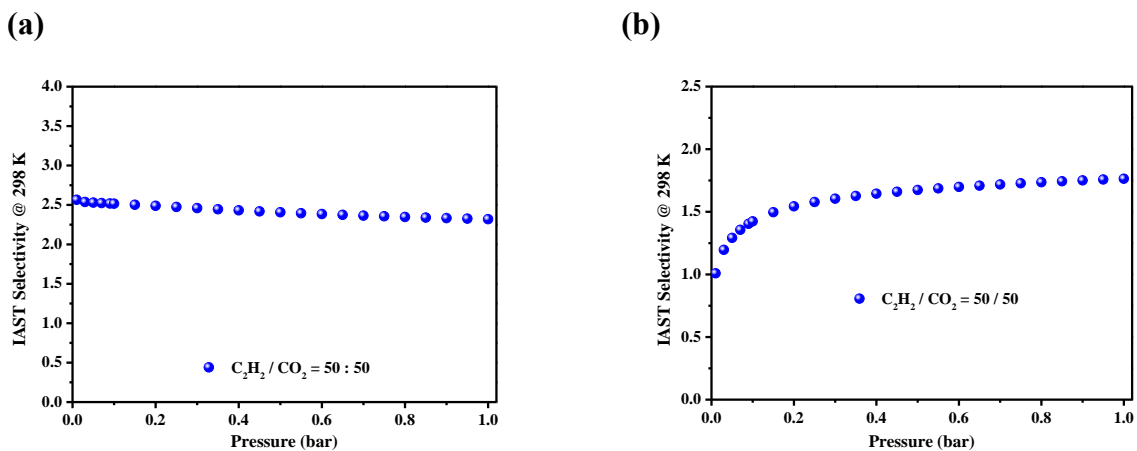


Fig. S22 Acetylene/carbon dioxide IAST selectivity of (a) Tb-NTB-HNTB and (b) Tb-NTB-BDC.

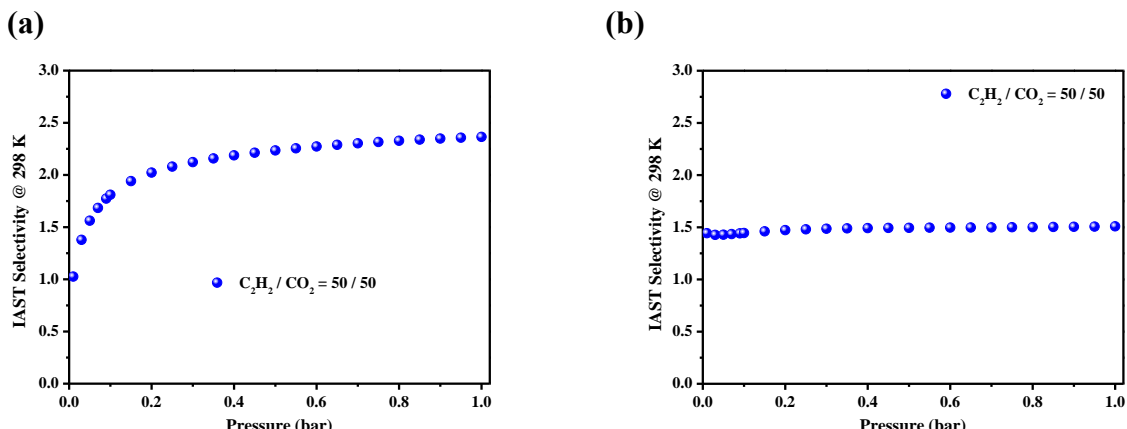


Fig. S23 Acetylene/carbon dioxide IAST selectivity of (a) Tb-NTB-1,4-NDC and (b) Tb-NTB-DTTDC.

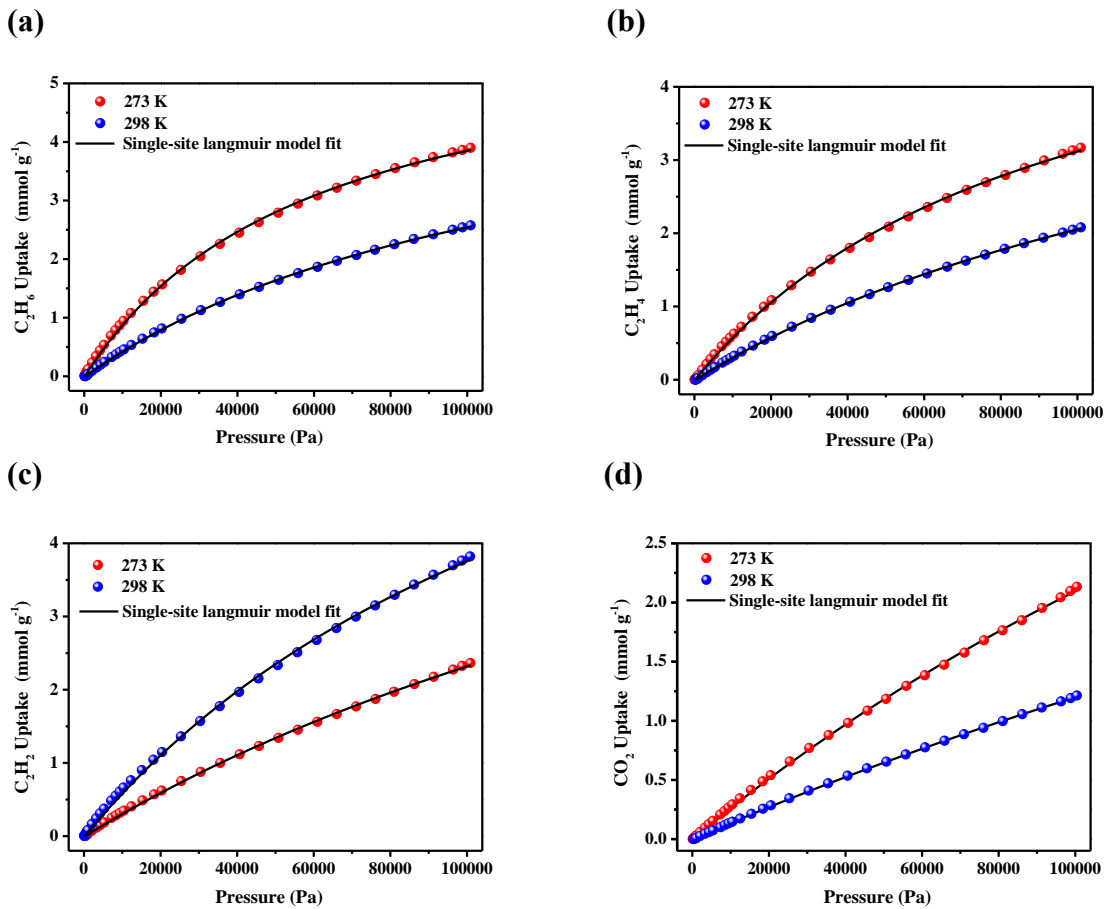


Fig. S24 Single-site Langmuir (SSL) model fitting (lines) of C_2H_6 , C_2H_4 , C_2H_2 and CO_2 adsorption isotherms (points) for Tb-NTB-HNTB measured at 273 and 298 K.

Table S1. The obtained SSL model fitting parameters of different gases for Tb-NTB-HNTB.

Tb-NTB-HNTB								
	C_2H_6		C_2H_4		C_2H_2		CO_2	
T (K)	273	298	273	298	273	298	273	298
Q	6.14275	5.66819	6.06458	5.61515	9.30849	8.45261	9.18854	8.23784
b	1.68511E-5	8.16234E-6	1.06056E-5	5.78079E-6	6.77355E-6	3.78677E-6	9.18854	1.70789E-6
R^2	0.9996	0.9998	0.9997	0.99991	0.9994	0.9995	0.9997	0.99993

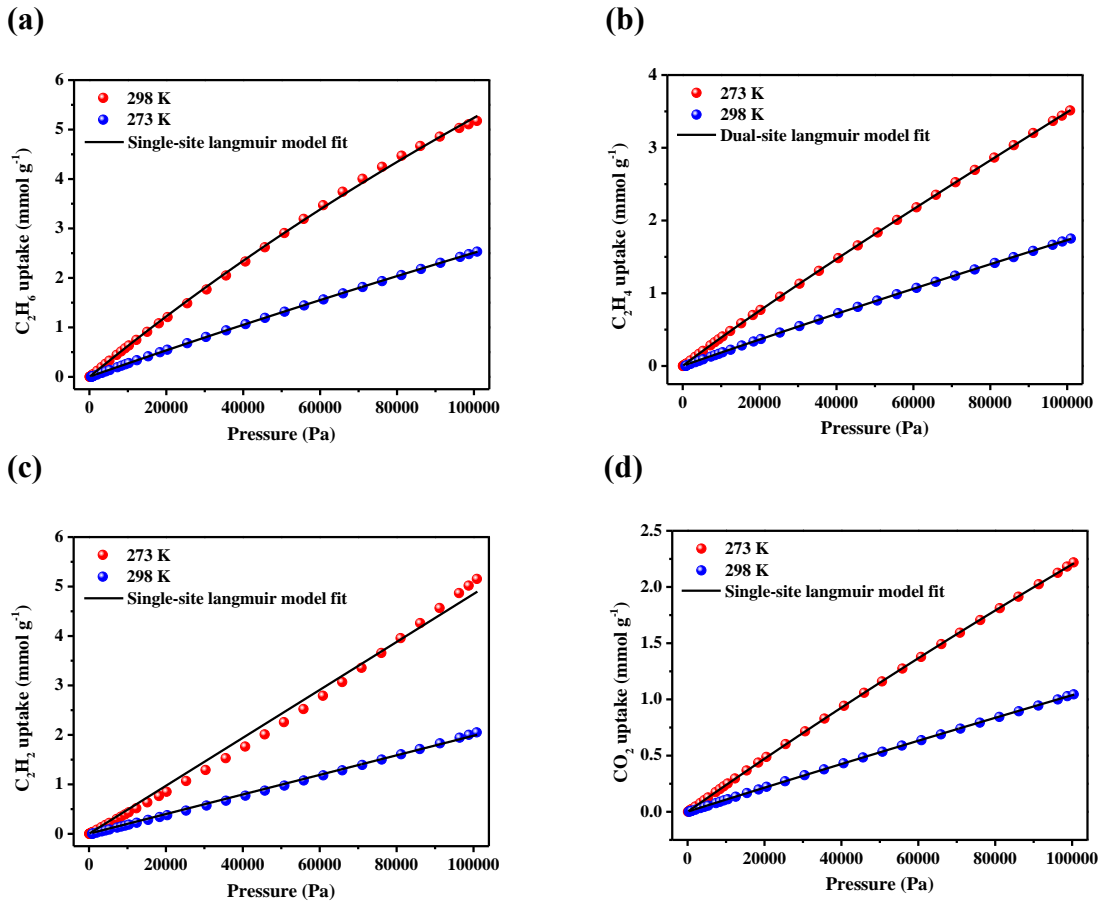


Fig. S25 Single/dual-site Langmuir model fitting (lines) of C_2H_6 , C_2H_4 , C_2H_2 and CO_2 adsorption isotherms (points) for Tb-NTB-BDC measured at 273 and 298 K.

Table S2. The obtained SSL model fitting parameters of different gases for Tb-NTB-BDC.

Tb-NTB-BDC						
	C_2H_6		C_2H_2		CO_2	
T (K)	273	298	273	298	273	298
Q	29.313	34.2567	52441.7	12803.2	26.5724	28.4074
b	2.17561E-6	7.8937E-7	9.24993E-10	1.54744E-9	9.03594E-7	3.78723E-7
R^2	0.9996	0.99994	0.995	0.999	0.99998	0.99995

Table S3. The obtained dual-site Langmuir (DSL) model fitting parameters of C_2H_4 for Tb-NTB-BDC.

Tb-NTB-BDC_ C_2H_4					
T (K)	Q_1	Q_2	b_1	b_2	R_2
273	0.300215	227.853	2.34348E-5	1.46065E-7	0.99999
298	2.08892	179.478	2.32848E-6	7.49329E-8	0.99990

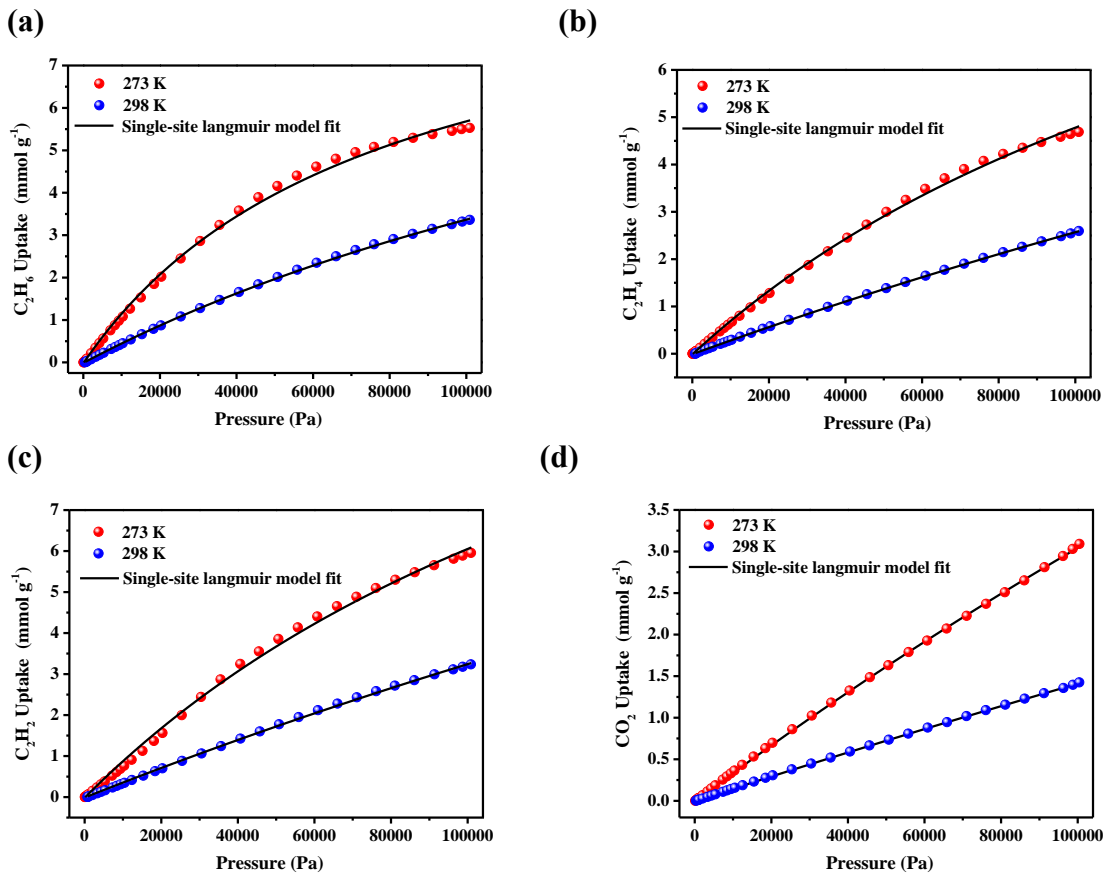
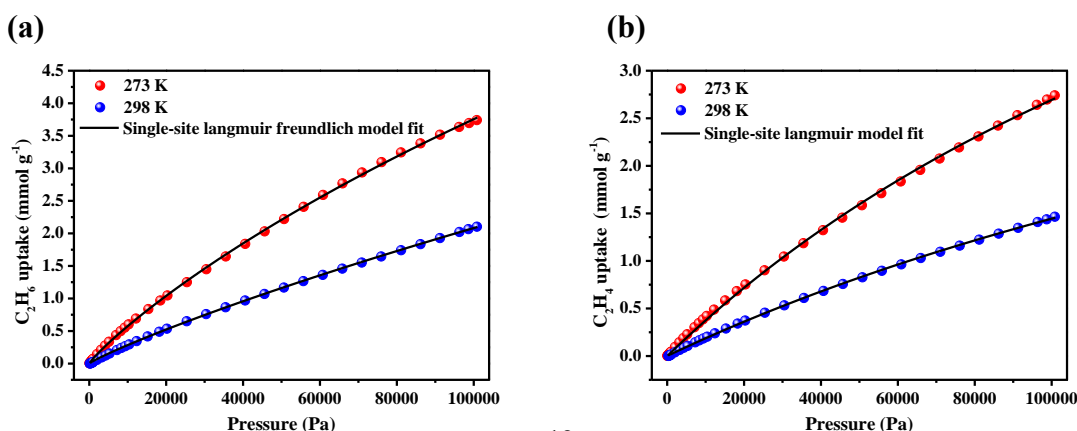


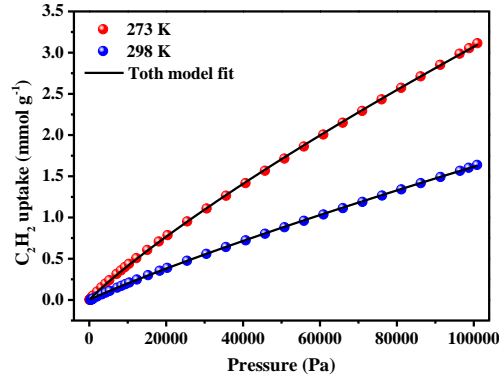
Fig. S26 SSL model fitting (lines) of C_2H_6 , C_2H_4 , C_2H_2 and CO_2 adsorption isotherms (points) for Tb-NTB-1,4-NDC measured at 273 and 298 K.

Table S4. The obtained SSL model fitting parameters of different gases for Tb-NTB-1,4-NDC.

Tb-NTB-1,4-NDC								
T (K)	C_2H_6		C_2H_4		C_2H_2		CO_2	
	273	298	273	298	273	298	273	298
Q	10.0167	11.5592	13.3751	20.9562	17.1142	26.6031	25.8809	23.5291
b	1.31512E-5	4.12169E-6	5.57164E-6	1.40188E-6	5.48183E-6	1.39206E-6	1.33496E-6	6.38956E-6
R^2	0.998	0.9997	0.999	0.9999	0.998	0.9993	0.9999	0.99997



(c)



(d)

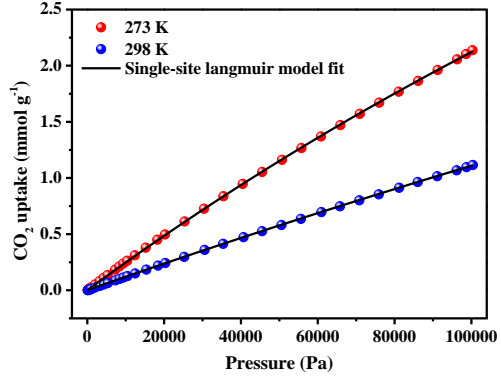


Fig. S27 Different model fitting (lines) of C₂H₆, C₂H₄, C₂H₂ and CO₂ adsorption isotherms (points) for Tb-NTB-DTTDC measured at 273 and 298 K.

Table S5. The obtained single-site Langmuir-Freundlich (SSLF) model fitting parameters of C₂H₆ for Tb-NTB-DTTDC.

Tb-NTB-DTTDC_C ₂ H ₆				
T (K)	<i>Q</i>	<i>b</i>	<i>t</i>	<i>R</i> ²
273	21.3703	7.82936E-6	1.12739	0.9998
298	25.9424	2.76738E-6	1.11149	0.9998

Table S6. The obtained Toth model fitting parameters of C₂H₂ for Tb-NTB-DTTDC.

Tb-NTB-DTTDC_C ₂ H ₂				
T (K)	<i>Q</i>	<i>b</i>	<i>t</i>	<i>R</i> ²
273	1936.27	3.03859E-8	0.27882	0.99992
298	441.305	5.28891E-8	0.368046	0.99993

Table S7. The obtained SSL model fitting parameters of C₂H₄ and CO₂ for Tb-NTB-DTTDC.

T (K)	Tb-NTB-DTTDC			
	C ₂ H ₄	CO ₂		
273	298	273	298	
<i>Q</i>	8.61675	5.8366	13.5173	14.3346
<i>b</i>	4.54529E-6	3.28571E-6	1.86159E-6	8.37804E-7
<i>R</i> ²	0.9995	0.9998	0.99996	0.99999

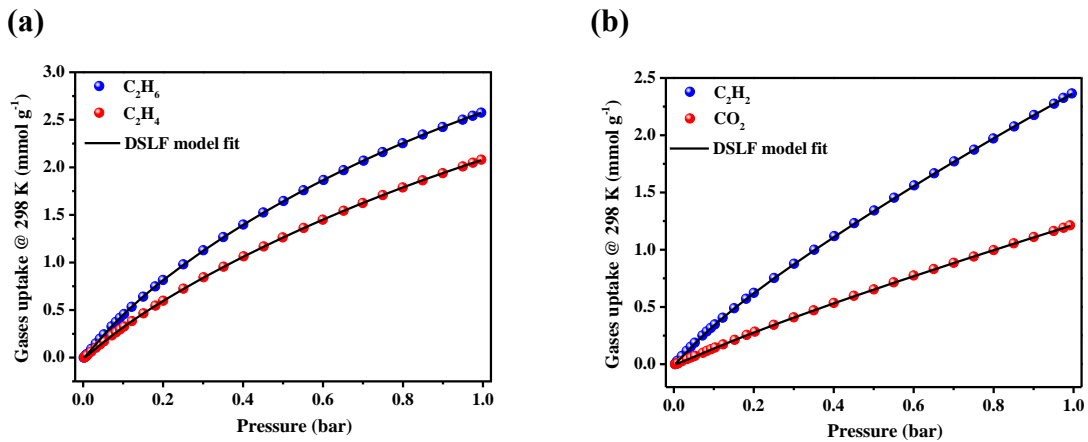


Fig. S28 Dual-site Langmuir-Freundlich (DSLF) equation fits (lines) and adsorption isotherms (points) of different gases at 298 K for Tb-NTB-HNTB.

Table S8. DSLF equation fitting parameters of different gases adsorption isotherms for Tb-NTB-HNTB.

Tb-NTB-HNTB				
gases	C ₂ H ₆	C ₂ H ₄	C ₂ H ₂	CO ₂
$q_{m,1}$	0.420846071691397	5.03519176203756	13.0056903440927	0.298001486765098
$q_{m,2}$	5.15241978055003	0.279146171810375	0.340210682583206	9.85033945385185
b_1	0.0513874748946263	0.00279510840481467	0.00122721449344107	0.020774672279944
b_2	0.00346658078881192	0.0443988866234479	0.0479070868700344	0.000501974391862696
n_1	1.26462134082121	1.15304243244317	1.09020923329425	1.14296683549559
n_2	1.16323559673573	1.28344968940332	1.18939053111837	1.16892137160416
<i>Reduced Chi-Sqr</i>	0.0109265540216912	0.00728418092232908	0.0105203873193918	0.00553066167357095
R^2	0.999991655279612	0.999991930145717	0.999989169429934	0.999980516309631

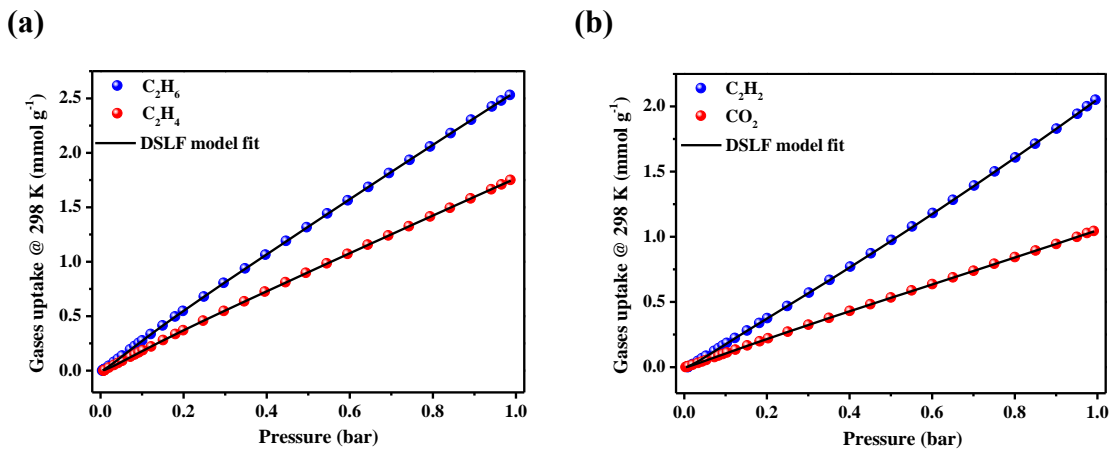


Fig. S29 DSLF equation fits (lines) and adsorption isotherms (points) of different gases at 298 K for Tb-NTB-BDC.

Table S9. DSLF equation fitting parameters of different gases adsorption isotherms for Tb-NTB-BDC.

gases	Tb-NTB-BDC			
	C ₂ H ₆	C ₂ H ₄	C ₂ H ₂	CO ₂
$q_{m,1}$	0.327233840215966	12.6652464750874	0.185164661537376	0.433693202297006
$q_{m,2}$	17.1194375909266	0.278040401847284	67.1609048604896	169.648371369297
b_1	0.0287217115678155	0.000440082073102288	0.0210629070509327	0.0152746992353958
b_2	0.00056724949729822	0.0217831221646556	0.0000960301693313378	0.000012798646278699
n_1	1.29334725390801	1.2428367188978	1.43012985099801	1.07376488635654
n_2	1.21216486751986	1.30306133620069	1.23616664927746	1.26922361080483
<i>Reduced Chi-Sqr</i>	0.00825625505281445	0.0130135411239726	0.0147442926248288	0.000579008163234031
R^2	0.99999468239069	0.999980212158248	0.999982807182008	0.999990186464511

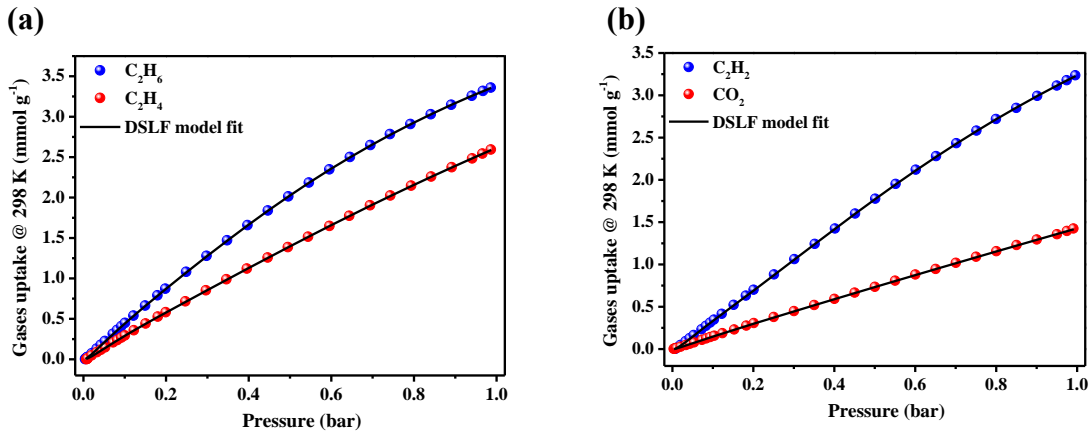


Fig. S30 DSLF equation fits (lines) and adsorption isotherms (points) of different gases at 298 K for Tb-NTB-1,4-NDC.

Table S10. DSLF equation fitting parameters of different gases adsorption isotherms for Tb-NTB-1,4-NDC.

gases	Tb-NTB-1,4-NDC			
	C ₂ H ₆	C ₂ H ₄	C ₂ H ₂	CO ₂
$q_{m,1}$	5.23090428247555	0.247025362597105	0.272834328684922	14.4045704161387
$q_{m,2}$	0.592278125755337	8.20010477889055	6.51054329158239	0.0785178486599558
b_1	0.00101273592815756	0.0356630931589339	0.038641633896936	0.000667224525439433
b_2	0.0427849251802233	0.00106458673722291	0.000964277903800458	0.0316020147723429
n_1	1.52930533501073	1.46959028139296	1.54364622849256	1.09421538154672
n_2	1.29665877304217	1.28960098894832	1.46703363797057	1.336735588448
<i>Reduced Chi-Sqr</i>	0.00457077748626839	0.0164677640982831	0.00598976286656235	0.000201853455599139
R^2	0.999995705941814	0.99998336961172	0.999991867252086	0.99998542115335

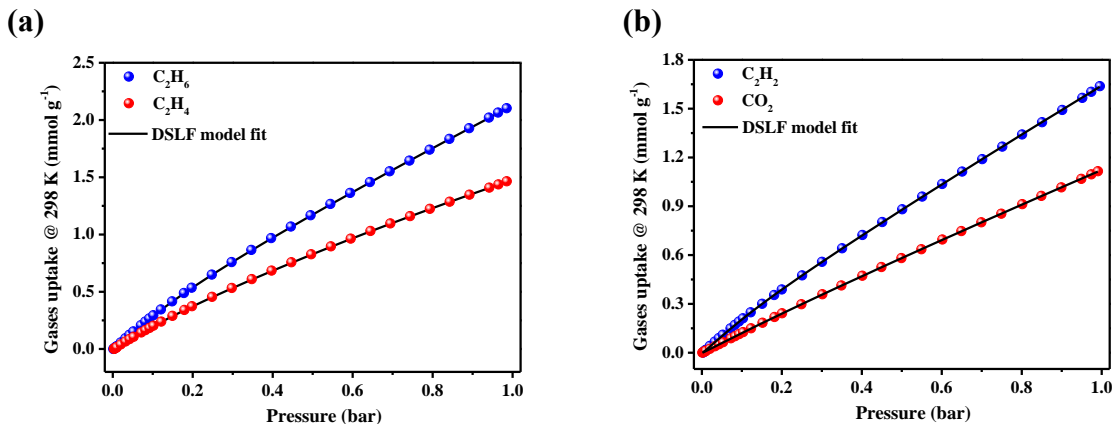


Fig. S31 DSLF equation fits (lines) and adsorption isotherms (points) of different gases at 298 K for Tb-NTB-DTTDC.

Table S11. DSLF equation fitting parameters of different gases adsorption isotherms for Tb-NTB-DTTDC.

Tb-NTB-DTTDC				
gases	C ₂ H ₆	C ₂ H ₄	C ₂ H ₂	CO ₂
$q_{m,1}$	18.4851260543874	6.51714315058874	0.234510916139449	0.393201421985735
$q_{m,2}$	0.447079838812974	0.201324518299416	17.5815468698429	8.57369132550398
b_1	0.000555128928795798	0.00138214040896643	0.0387713820674364	0.022089681501044
b_2	0.034693339500298	0.041558369981383	0.000527961168941006	0.000342717928022305
n_1	1.13310442340014	1.12454177580067	1.16651999973779	0.979204435496264
n_2	1.16271511626126	1.20807790794357	1.11007548404262	1.25354454619881
<i>Reduced Chi-Sqr</i>	0.00574301582562789	0.00451624218950283	0.00538680902501112	0.000416185955404125
R^2	0.99999432988281	0.999991671397619	0.999991446859797	0.999997123906926

Section 6. High-Pressure Methane Sorption Measurements

High-pressure excess methane sorption isotherms were measured with an automatic volumetric sorption apparatus (BELSORP-HP) in the range of 0-80 bar. The bath temperature for CH₄ sorption measurements was controlled using a recirculating bath containing an ethylene glycol/H₂O mixture. Ultrahigh purity He was used to determine the dead space of the sample cell. The sorption data were corrected to give the final gravimetric excess sorption isotherm $n_{ex}(P, T)$, by subtracting the background sorption measured with the empty sample cell using the same test parameters. The total sorption, which represents the real gas-storage performance of the porous material but cannot be directly measured, was calculated by [Eqn. 8]:

$$n_{tot}(P, T) = n_{ex}(P, T) + \rho_{gas}(P, T) \times V_p \quad (8)$$

Where $\rho_{gas}(P, T)$ is the density of bulk methane at pressure P and temperature T , and V_p is the pore volume of the porous material determined from N₂ adsorption isotherm at 77 K.

The isosteric enthalpy of adsorption, Q_{st} for methane was determined by fitting the adsorption isotherms at 273 and 298 K to the Dual-site Langmuir equation (Eqn 3);

Using the Dual-site Langmuir fit, the isosteric heat of adsorption can be calculated for the material as a function of the total amount of methane adsorbed using the Clausius-Clapeyron relation (Eqn 2).

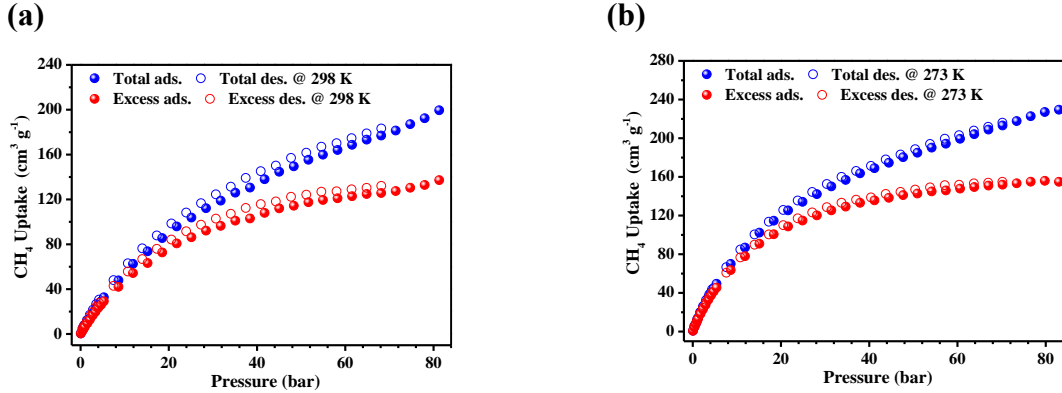


Fig. S32 High-pressure CH₄ sorption isotherms for Tb-NTB-DTTDC at (a) 298 K and (b) 273 K, respectively.

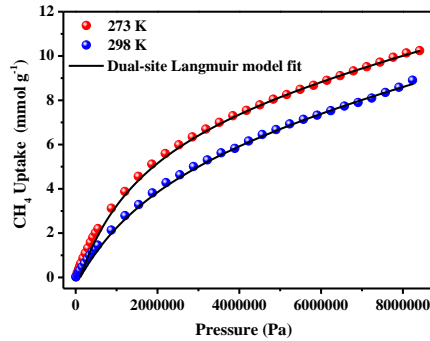


Fig. S33 DSL model fitting (lines) of CH₄ adsorption isotherms (points) for Tb-NTB-DTTDC measured at 273 and 298 K.

Table S12. The obtained DSL model fitting parameters for Tb-NTB-DTTDC.

T (K)	$n_{L,A}$	$n_{L,B}$	b_A	b_B	R^2
273	2412.59	8.29488	1.6518E-10	5.88412E-7	0.999937
298	7.13986	1939.48	3.97923E-7	2.05572E-10	0.99979

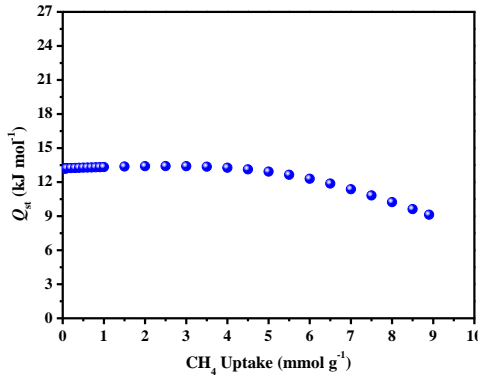


Fig. S34 Heats of CH₄ adsorption (Q_{st}) for Tb-NTB-DTTDC, which were calculated from the Dual-site Langmuir model fitting of adsorption isotherms at 273 and 298 K as a function of the total CH₄ uptake amount using the Clausius-Clapeyron equation:

$$\frac{dlnp}{dT} = \frac{\Delta H}{nRT^2} = \frac{\Delta_r H_m}{RT^2}.$$

Section 7. Single Crystal X-ray Crystallography Data

Single-crystal X-ray diffraction data for Tb-NTB-HNTB, Tb-NTB-BDC, Tb-NTB-1,4-NDC, Tb-NTB-DTTDC and Tb-NTB-OBDC were collected on a Bruker D8 venture diffractometer ($\text{Cu}/K\alpha$, $\lambda = 1.54178 \text{ \AA}$) at 243 K. Indexing was performed using APEX3 (Difference Vectors method).⁶ Data integration and reduction were performed using SaintPlus 6.01.⁷ Absorption correction was performed by multi-scan method implemented in SADABS.⁸ Space group was determined using XPREP implemented in APEX3. The structure was solved by direct methods and refined with full-matrix least squares technique using the SHELXT⁹ package or refined using SHELXL-2014 (full-matrix least-squares on F^2) contained in Olex2.¹⁰ Non-hydrogen atoms were refined with anisotropic displacement parameters during the final cycles. Hydrogen atoms were located at geometrically calculated positions to their carrier atoms and refined with isotropic thermal parameters included in the final stage of the refinement. For these compounds, the contributions of heavily disordered solvent molecules were treated as diffuse using Squeeze procedure implemented in Platon program.¹¹⁻¹³

A summary of the crystallographic data is given in Table S13-17. CCDC 2235992-2235996 (Tb-NTB-HNTB, Tb-NTB-BDC, Tb-NTB-1,4-NDC, Tb-NTB-DTTDC and Tb-NTB-OBDC) contain the supplementary crystallographic data for this paper. These data can be obtained free of charge from The Cambridge Crystallographic Data Centre.

Table S13. Crystal data and refinement results for Tb-NTB-HNTB.

Identification code	Tb-NTB-HNTB
Empirical formula	C ₄₂ H ₂₄ N ₂ O ₁₇ F ₄ Tb ₃
Formula weight	1381.42
Temperature/K	243.0
Wavelength/Å	1.54178
Crystal system	Monoclinic
Space group	<i>C2/m</i>
Unit cell dimensions/Å	$a = 18.018(2)$ $b = 31.261(4)$ $c = 17.687(3)$ $\beta/\circ = 111.754(7)$
Volume/Å ³	9253(2)
Z	4
Density (calculated)/Mg/m ³	0.992
Absorption coefficient/mm ⁻¹	11.473
F (000)	2628.0
Crystal size/mm ³	0.16 × 0.08 × 0.08
Theta range for data collection/°	4.963 to 51.755
Index ranges	-18<=h<=18 -31<=k<=30 -17<=l<=17
Reflections collected	17740
Independent reflections	4968 [$R_{\text{int}} = 0.0663$]
Completeness to theta = 51.755°	94.5%
Refinement method	Full-matrix least-squares on F^2
Data / restraints / parameters	4968 / 559 / 293
Goodness-of-fit on F^2	1.119
Final <i>R</i> indices [$I > 2\sigma(I)$]	$R_1 = 0.0888$, $wR_2 = 0.2528$
<i>R</i> indices (all data)	$R_1 = 0.0983$, $wR_2 = 0.2721$
Largest diff. peak and hole/e.Å ⁻³	2.05 and -2.43

Table S14. Crystal data and refinement results for Tb-NTB-BDC.

Identification code	Tb-NTB-BDC
Empirical formula	C ₃₃ H ₁₈ NO ₁₂ F ₄ Tb ₃
Formula weight	1173.27
Temperature/K	243.0
Wavelength/Å	1.54178
Crystal system	Hexagonal
Space group	<i>P</i> 6 ₃ / <i>mcm</i>
Unit cell dimensions/Å	$a = 18.0166(4)$ $c = 27.4264(6)$
Volume/Å ³	7709.8(4)
Z	4
Density (calculated)/Mg/m ³	1.011
Absorption coefficient/mm ⁻¹	13.639
F (000)	2200.0
Crystal size/mm ³	0.08 × 0.08 × 0.03
Theta range for data collection/°	4.29 to 54.238
Index ranges	-17<=h<=18 -16<=k<=18 -28<=l<=25
Reflections collected	17728
Independent reflections	1719 [$R_{\text{int}} = 0.0343$]
Completeness to theta = 54.238°	99.4%
Refinement method	Full-matrix least-squares on F^2
Data / restraints / parameters	1719 / 12 / 90
Goodness-of-fit on F^2	1.135
Final <i>R</i> indices [$I > 2\sigma(I)$]	$R_1 = 0.0582$, $wR_2 = 0.1861$
<i>R</i> indices (all data)	$R_1 = 0.0624$, $wR_2 = 0.1916$
Largest diff. peak and hole/e.Å ⁻³	1.89 and -1.75

Table S15. Crystal data and refinement results for Tb-NTB-1,4-NDC.

Identification code	Tb-NTB-1,4-NDC
Empirical formula	C ₄₅ H ₂₁ N ₄ O ₁₅ F ₄ Tb ₃
Formula weight	1431.58
Temperature/K	243.0
Wavelength/Å	1.54178
Crystal system	Hexagonal
Space group	<i>P</i> 6 ₃ / <i>mcm</i>
Unit cell dimensions/Å	<i>a</i> = 18.0378(4) <i>c</i> = 27.5886(6)
Volume/Å ³	7773.7(4)
Z	4
Density (calculated)/Mg/m ³	1.223
Absorption coefficient/mm ⁻¹	13.657
F (000)	2764.0
Crystal size/mm ³	0.08 × 0.08 × 0.04
Theta range for data collection/°	5.159 to 54.235
Index ranges	-18<=h<=17 -18<=k<=18 -28<=l<=29
Reflections collected	16985
Independent reflections	1681 [<i>R</i> _{int} = 0.0328]
Completeness to theta = 54.235°	96.9%
Refinement method	Full-matrix least-squares on <i>F</i> ²
Data / restraints / parameters	1681 / 348 / 189
Goodness-of-fit on <i>F</i> ²	1.183
Final <i>R</i> indices [<i>I</i> >2sigma(<i>I</i>)]	<i>R</i> ₁ = 0.0583, <i>wR</i> ₂ = 0.1806
<i>R</i> indices (all data)	<i>R</i> ₁ = 0.0621, <i>wR</i> ₂ = 0.1852
Largest diff. peak and hole/e.Å ⁻³	1.25 and -0.82

Table S16. Crystal data and refinement results for Tb-NTB-DTTDC.

Identification code	Tb-NTB-DTTDC
Empirical formula	C ₃₆ H ₁₅ NO ₁₅ S _{4.5} F ₄ Tb ₃
Formula weight	1404.57
Temperature/K	243.0
Wavelength/Å	1.54178
Crystal system	Hexagonal
Space group	<i>P</i> 6 ₃ / <i>mcm</i>
Unit cell dimensions/Å	<i>a</i> = 17.8807(6) <i>c</i> = 34.2217(14)
Volume/Å ³	9475.5(7)
Z	4
Density (calculated)/Mg/m ³	0.985
Absorption coefficient/mm ⁻¹	12.092
F (000)	2668.0
Crystal size/mm ³	0.1 × 0.1 × 0.05
Theta range for data collection/°	2.582 to 50.460
Index ranges	-13 ≤ <i>h</i> ≤ 15 -17 ≤ <i>k</i> ≤ 16 -34 ≤ <i>l</i> ≤ 34
Reflections collected	25841
Independent reflections	1820 [<i>R</i> _{int} = 0.0596]
Completeness to theta = 50.460°	99.9%
Refinement method	Full-matrix least-squares on <i>F</i> ²
Data / restraints / parameters	1820 / 273 / 180
Goodness-of-fit on <i>F</i> ²	1.068
Final <i>R</i> indices [<i>I</i> >2sigma(<i>I</i>)]	<i>R</i> ₁ = 0.0750, <i>wR</i> ₂ = 0.2030
<i>R</i> indices (all data)	<i>R</i> ₁ = 0.0812, <i>wR</i> ₂ = 0.2082
Largest diff. peak and hole/e.Å ⁻³	1.18 and -0.70

Table S17. Crystal data and refinement results for Tb-NTB-OBDC.

Identification code	Tb-NTB-OBDC
Empirical formula	C ₄₅ H ₂₄ N ₄ O ₁₈ F ₄ Tb ₃
Formula weight	1461.47
Temperature/K	243.0
Wavelength/Å	1.54178
Crystal system	Trigonal
Space group	<i>P</i> -31 <i>m</i>
Unit cell dimensions/Å	18.0964(8) 15.2035(6)
Volume/Å ³	4311.8(4)
Z	2
Density (calculated)/Mg/m ³	1.126
Absorption coefficient/mm ⁻¹	12.353
F (000)	1394.0
Crystal size/mm ³	0.12 × 0.12 × 0.06
Theta range for data collection/°	5.646 to 50.49
Index ranges	-17 ≤ h ≤ 18 -18 ≤ k ≤ 16 -15 ≤ l ≤ 15
Reflections collected	12979
Independent reflections	1618 [$R_{\text{int}} = 0.1067$]
Completeness to theta = 50.490°	99.2%
Refinement method	Full-matrix least-squares on F^2
Data / restraints / parameters	1618 / 69 / 135
Goodness-of-fit on F^2	1.044
Final <i>R</i> indices [$I > 2\sigma(I)$]	$R_1 = 0.0714$, $wR_2 = 0.1855$
<i>R</i> indices (all data)	$R_1 = 0.0778$, $wR_2 = 0.1892$
Largest diff. peak and hole/e.Å ⁻³	1.27 and -1.03

Section 8. References

1. S. Nandi, D. Chakraborty and R. Vaidhyanathan, *Chem. Commun.*, 2016, **52**, 7249-7252.
2. B. T. Nguyen, H. L. Nguyen, T. C. Nguyen, K. E. Cordova and H. Furukawa, *Chem. Mater.*, 2016, **28**, 6243-6249.
3. A. L. Myers, J. M. Prausnitz, *AIChE J.*, 1965, **11**, 121.
4. Y. S. Bae, K. L. Mulfort, H. Frost, P. Ryan, S. Punnathanam, L. J. Broadbelt, J. T. Hupp, R. Q. Snurr, *Langmuir*, 2008, **24**, 8592
5. B. Mu, F. Li, K. S. Walton, *Chem. Commun.*, 2009, 2493.
6. Bruker APEX2; Bruker AXS, Inc.: Madison, WI, 2010.
7. Bruker SAINT, Data Reduction Software; Bruker AXS, Inc.: Madison, WI, 2009.
8. G. M. Sheldrick, University of Gottingen: Gottingen, Germany, 1996.
9. G. M. Sheldrick, *Acta Crystallogr.*, 2015, **A71**, 3-8.
10. O. V. Dolomanov, L. J. Bourhis, R. J. Gildea, J. A. K. Howard, H. Puschmann, *J. Appl. Crystallogr.*, 2009, **42**, 339-341.
11. A. L. Spek, *Acta Crystallogr.*, 1990, **A46**, 194-201.
12. A. L. Spek, *J. Appl. Crystallogr.*, 2003, **36**, 7-13.
13. A. L. Spek, *Acta Crystallogr.*, 2009, **D65**, 148-155.